Theoretical Study on Photophysical Properties of Ambipolar Spirobifluorene Derivatives as Efficient Blue-Light-Emitting Materials

Xue-Qin Ran,* Ji-Kang Feng,* Ai-Min Ren, Wen-Chao Li, Lu-Yi Zou, and Chia-Chung Sun

State Key Laboratory of Theoretical and Computational Chemistry, Institute of Theoretical Chemistry, Jilin University, Changchun 130023, People's Republic of China

Received: April 16, 2009; Revised Manuscript Received: May 23, 2009

The aim of this work is to provide an in-depth interpretation of the optical and electronic properties of a series of spirobifluorene derivatives. These materials show great potential for application in organic light-emitting diodes as efficient blue-light-emitting materials due to the tuning of the optical and electronic properties by the use of different electron donors (D) and electron acceptors (A). The geometric and electronic structures of the molecules in the ground state are studied with density functional theory (DFT) and ab initio HF, whereas the lowest singlet excited states are optimized by ab initio CIS. The energies of the lowest singlet excited states are calculated by employing time-dependent density functional theory (TD-DFT). The results show that the HOMOs, LUMOs, energy gaps, ionization potentials, electron affinities, reorganization energies, and exciton binding energies for these complexes are affected by different D and A moieties. Also, it has obtained that these blue-light-emitting materials have improved charge transport rate and charge transfer balance performance and can be used as efficient ambipolar-transporting materials in organic light-emitting diodes.

1. Introduction

In the process of fabricating single-layer organic light-emitting devices (OLEDs), continuous efforts have been devoted to the development of more efficient and high-performance light-emitting materials. Among these materials, 9,9′-spirobifluorene-cored compounds have received considerable attention.[1] By tailoring the nature of the substituents and their substitution patterns about the 9,9′-spirobifluorene unit, for example, with an identical or different biphenyl branch,[2,3] it is easy to manipulate the electronic structure, emission spectrum, thermal/morphological stability, or charge carrier mobility of 9,9′-spirobifluorene-based materials. Moreover, with developing emitters equipped with an appropriate electron donor (D) that facilitates hole injection and/or transport and an electron acceptor (A) that improves electron injection and/or transport,[4] it is promising to balance the electron−hole recombination efficiency, to control the levels of the highest occupied molecular orbital (HOMO) and lowest unoccupied molecular orbital (LUMO) as well as the emission color to a fine degree,[5−8] making such systems increasingly attractive for use in single-layer OLEDs.[9−11] However, the 9,9′-spirobifluorene derivatives featuring donors on one biphenyl branch spiro-linked to another biphenyl moiety bearing acceptors exhibit low photoluminescence efficiencies as a result of strong photoinduced electron transfer.[12,13] As a result, a better alternative is to position the D and A moieties on the same biphenyl branch of the spirobifluorene.

Recently, Wong et al. have synthesized an efficient spiro-configured D−A bipolar blue-light-emitting material, 2,2′-bis(diphenylamino)-7,7′-bis(diphenylbenzimidazole)-9,9′-spirobifluorene, which exhibits high thermal stability, multifunctional properties, and has promising potential for application in OLEDs.[14] Therefore, it is significant for us to study this molecule (3) theoretically, together with two other molecules, 2,2′-bis(diphenylamino)-9,9′-spirobifluorene (1) and 7,7′-bis(diphenylbenzimidazole)-9,9′-spirobifluorene (2). To search for new blue-light-emitting materials with improved charge-transfer/injection performance, two complexes were designed and investigated here, 2,2′-bis(diphenylamino)-7,7′-bis(benzimidazole)-9,9′-spirobifluorene (4) and 2,2′-bis(diphenylamino)-7,7′-bis(nitryl)-9,9′-spirobifluorene (5). Density functional theory (DFT), the singles configuration interaction (CIS) methods, and time-dependent density functional theory (TD-DFT) calculations have been carried out for the considered molecules. Particular attention was paid to the influence of different D and A moieties. HOMOs, LUMOs, energy gaps, ionization potentials (IPs), electron affinities (EAs), reorganization energies (λs), exciton binding energies (E_bs), and molecular modeling of these molecules indicate that 3, 4, and 5 show improved OLED device performance as blue-light-emitting materials.

2. Computational Details

All calculations on the considered molecules have been performed on the SGI origin 2000 server with the *Gaussian 03* program package.[15] The ground-state geometries as well as the cationic and anionic structures of the studied molecules were optimized by DFT//B3LYP/6-31G(d). There is no symmetric constraint on the geometric optimization. The isomers of the studied molecules were considered and the molecular geometry with the lowest energy was selected for further investigations. CIS/3-21G(d) were employed to calculate the lowest singlet excited state geometries based on the optimized geometries obtained from HF/3-21G(d). The electronic absorption and emission spectra were systematically investigated by the TD-DFT method on the basis of each optimized structure. In addition, the various properties of these molecules, such as highest occupied molecular orbitals (HOMOs), lowest unoccupied molecular orbitals (LUMOs), energy gaps, ionization potentials (IPs), electron affinities (EAs), reorganization ener-

* To whom correspondence is addressed. E-mail: jikangf@yahoo.com. Phone: +86-431-88499856Fax: +86-431-88498026.

10.1021/jp903511r CCC: $40.75
Published on Web 06/09/2009

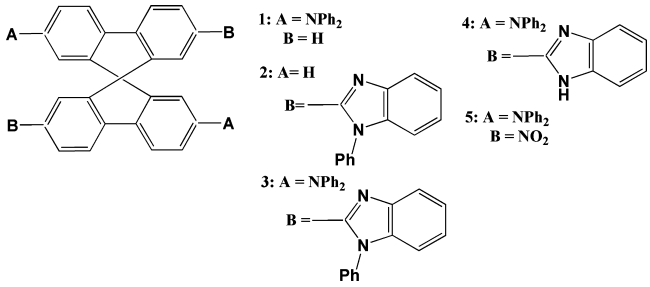

Figure 1. Sketch map of the structures of 1−5.

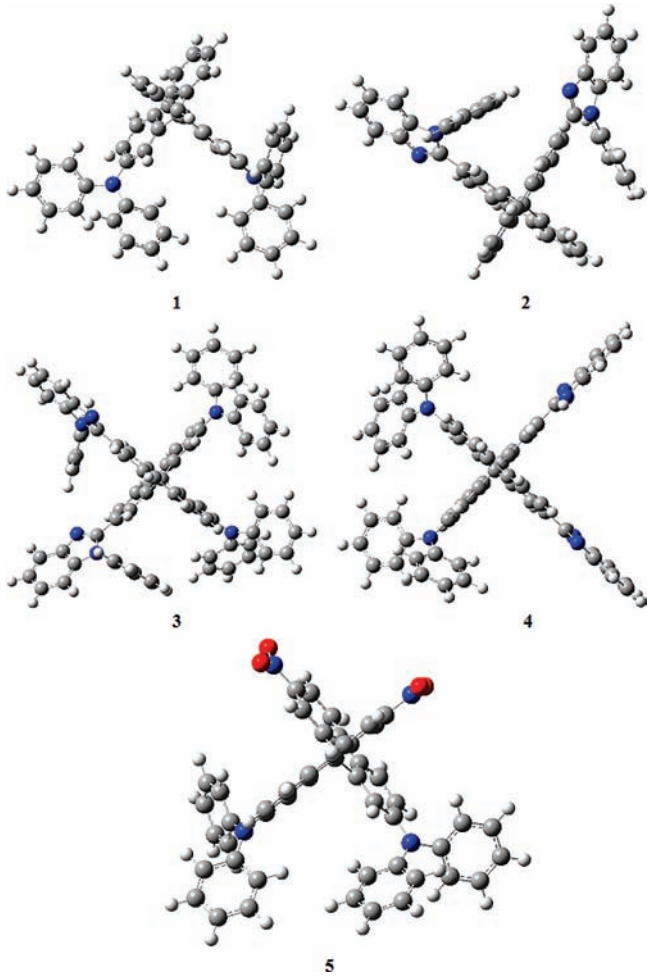

Figure 2. Optimized structures of 1−5 by DFT//B3LYP/6-31G(d).

gies, and exciton binding energies are obtained from the computed results and compared with the available experimental data.

3. Results and Discussion

3.1. Ground- and Excited-State Geometries. The sketch map of the structures is depicted in Figure 1, and the optimized geometries obtained by DFT//B3LYP/6-31G(d) of 1−5 are plotted in Figure 2. The selected bond lengths and bond angles of 1−5 calculated by DFT and HF are listed in Tables 1 and 2, separately. For the purpose of comparison of the ground- and excited-state geometries, a part of bond lengths and angles of the excited state structures for the considered molecules obtained by CIS/3-21G(d) are shown in Table 2, too.

As observed in Table 1, the DFT-calculated results show that different electron donors (D) and electron acceptors (A) lead to larger variations in bond lengths than in bond angles. For example, the bonds C(2)−C(3), C(3)−C(4), and C(2)−C(3) in 1−5 have the difference of 0.009, 0.011, and 0.007 Å. However, the bond angles in 1−5 have very small changes with different D and A moieties, about ∼0.1−0.2°. Additionally, the planes containing monofluorenes in 1−5 are orthogonal to each other. In the ground state, the DFT-calculated results are similar to those obtained with the HF approach, as shown in Tables 1 and 2.

TABLE 1: Selected Important Bond Lengths and Angles of 1−5 in the Ground State with DFT//B3LYP/6-31G(d)

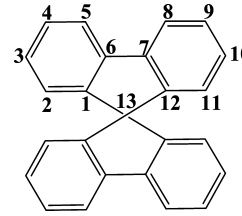

DFT	1	2	3	4	5
C(1)−C(2)	1.389	1.389	1.386	1.385	1.384
C(2)−C(3)	1.400	1.399	1.408	1.408	1.399
C(3)−C(4)	1.399	1.400	1.409	1.409	1.398
C(4)−C(5)	1.397	1.396	1.392	1.391	1.392
C(5)−C(6)	1.397	1.397	1.397	1.399	1.400
C(6)−C(1)	1.409	1.408	1.409	1.408	1.413
C(6)−C(7)	1.467	1.468	1.464	1.464	1.461
C(7)−C(8)	1.397	1.397	1.398	1.397	1.398
C(8)−C(9)	1.393	1.392	1.391	1.392	1.390
C(9)−C(10)	1.408	1.408	1.409	1.409	1.412
C(10)−C(11)	1.407	1.407	1.408	1.408	1.410
C(11)−C(12)	1.386	1.386	1.387	1.385	1.384
C(12)−C(7)	1.408	1.407	1.408	1.409	1.408
C(12)−C(13)	1.532	1.532	1.535	1.532	1.532
C(13)−C(1)	1.533	1.532	1.531	1.533	1.532
C(1)−C(6)−C(7)	108.6	108.6	108.8	108.7	108.7
C(6)−C(7)−C(12)	108.8	108.7	108.7	108.8	108.9
C(7)−C(12)−C(13)	110.6	110.7	110.6	110.6	110.6
C(12)−C(13)−C(1)	101.3	101.2	101.3	101.2	101.2
dipole moment (D)	0.21	4.52	5.04	3.28	10.07

As listed in Table 2, the comparison with HF-calculated results indicates that electronic excitation leads to the large variations of the spirobifluorene derivatives. For 1−5 in the excited state, the bonds C(1)−C(2), C(4)−C(5), C(6)−C(7), C(8)−C(9), and C(11)−C(12) are shortened, whereas bonds C(2)−C(3), C(3)−C(4), C(5)−C(6), C(6)−C(1), C(7)−C(8), C(9)−C(10), C(10)−C(11), and C(12)−C(7) are elongated. The bond angles change little (less than 1.2°). In addition, the dipole moments of 1−5 are calculated and listed in Tables 1 and 2. In the ground state, the HF data are higher than those calculated by DFT in 1 and 2, which is the reverse of that in 3, 4, and 5. With the exception of 1, the dipole moments of these materials are very large and this can be ascribed to the high 3D nonplanar molecular structures. Furthermore, we find that the dipole moments of the considered molecules in the excited state are all higher than that in the ground state calculated by HF, with a difference of 0.31−1.49 D.

3.2. Frontier Molecular Orbitals. For the sake of characterizing the optical and electronic properties, it is useful to examine the HOMOs, LUMOs, and energy gaps. To gain insight into the influence of the various D and A moieties in spirobifluorene derivatives, the plots of HOMOs and LUMOs for 1−5 obtained by DFT//B3LYP/6-31G(d) are showed in Figure 3. Table 3 lists the calculated HOMO and LUMO energies and energy gaps, as well as the available experimental results. To more easily and vividly observe the variations of the HOMOs, LUMOs, and

TABLE 2: Selected Important Bond Lengths and Angles of 1−5 in the Ground State with HF/3-21G(d) and in the Excited State with CIS/3-21G(d)[a]

	1	2	3	4	5
C(1)−C(2)	1.376, (1.369)[a]	1.376, (1.370)	1.374, (1.353)	1.374, (1.353)	1.369, (1.370)
C(2)−C(3)	1.388, (1.393)	1.388, (1.391)	1.392, (1.422)	1.391, (1.420)	1.384, (1.384)
C(3)−C(4)	1.386, (1.405)	1.387, (1.398)	1.393, (1.439)	1.393, (1.432)	1.380, (1.381)
C(4)−C(5)	1.387, (1.369)	1.386, (1.375)	1.382, (1.355)	1.381, (1.356)	1.382, (1.381)
C(5)−C(6)	1.382, (1.418)	1.382, (1.406)	1.383, (1.420)	1.384, (1.421)	1.384, (1.384)
C(6)−C(1)	1.394, (1.436)	1.394, (1.420)	1.393, (1.439)	1.393, (1.440)	1.398, (1.397)
C(6)−C(7)	1.476, (1.400)	1.476, (1.419)	1.474, (1.402)	1.474, (1.402)	1.471, (1.471)
C(7)−C(8)	1.381, (1.426)	1.382, (1.415)	1.381, (1.415)	1.381, (1.416)	1.382, (1.382)
C(8)−C(9)	1.384, (1.355)	1.382, (1.355)	1.383, (1.363)	1.383, (1.362)	1.381, (1.381)
C(9)−C(10)	1.391, (1.437)	1.392, (1.449)	1.392, (1.418)	1.393, (1.419)	1.396, (1.396)
C(10)−C(11)	1.392, (1.425)	1.392, (1.433)	1.392, (1.411)	1.393, (1.413)	1.395, (1.394)
C(11)−C(12)	1.374, (1.350)	1.374, (1.350)	1.374, (1.357)	1.373, (1.356)	1.373, (1.373)
C(12)−C(7)	1.393, (1.450)	1.393, (1.437)	1.393, (1.432)	1.393, (1.433)	1.392, (1.393)
C(12)−C(13)	1.528, (1.530)	1.527, (1.530)	1.527, (1.529)	1.528, (1.529)	1.528, (1.527)
C(13)−C(1)	1.529, (1.529)	1.529, (1.528)	1.529, (1.530)	1.529, (1.530)	1.527, (1.528)
C(1)−C(6)−C(7)	108.6, (109.6)	108.6, (109.6)	108.7, (109.5)	108.6, (109.4)	108.6, (108.5)
C(6)−C(7)−C(12)	108.8, (109.5)	108.7, (109.2)	108.7, (109.9)	108.8, (109.9)	108.9, (108.9)
C(7)−C(12)−C(13)	110.5, (109.4)	110.6, (109.4)	110.5, (109.6)	110.5, (109.6)	110.5, (110.5)
C(12)−C(13)−C(1)	101.6, (101.3)	101.5, (101.5)	101.5, (101.4)	101.5, (101.5)	101.5, (101.5)
dipole moment (D)	0.25, (0.73)	4.86, (5.17)	4.90, (5.96)	2.83, (3.73)	9.96, (11.45)

[a] The calculated results in the bracket are by CIS/3-21G(d).

energy gaps, the total density of states (DOS) of 1−5 have been compared with each other, as shown in Figure 4.

Here, the energy gap calculated in theory is the orbital energy difference between HOMO and LUMO, termed the HOMO−LUMO gap (ΔE_{H-L}).[16−18] Experimentally, the most used band gap is obtained from the absorption spectra, which is the lowest transition (or excitation) energy from the ground state to the first dipole-allowed excited state, termed the optical band gap (E_g). In fact, the optical band gap is not the orbital energy difference between HOMO and LUMO, but the energy difference between the S_0 and S_1 states. Only when the excitation to the S_1 state corresponds almost exclusively to the promotion of the electron from the HOMO to the LUMO can the optical band gap be approximately equal to the HOMO−LUMO gap in quantity. In this contribution, the optical band gaps of 1−5 were obtained from the absorption spectra by TD-DFT.

As observed in Figure 3, the frontier orbitals show π characteristics. For 1−5, the HOMO orbitals are spread over the spirobifluorene cores and diphenylamino, but the LUMO orbitals are mainly centralized on the spirobifluorene cores. In general, the HOMO orbitals exhibit bonding character and the LUMO orbitals hold antibonding character. It is worth noting that the HOMO orbitals show an antibonding interaction between the two adjacent subunits, and the LUMO orbitals represent the bonding interaction in these regions, consistent with the shortening of the corresponding inter-ring bond lengths in the excited states. Importantly, because the lowest singlet excited state corresponds almost exclusively to the excitation from the HOMO to the LUMO in all studied molecules (Absorption and Emission Spectra section), we can predict the differences of the bond lengths between the ground (S_0) and lowest singlet excited state (S_1) from MO nodal patterns. For example, the HOMO orbitals of the studied molecules have nodes across the C(1)−C(2), C(4)−C(5), C(6)−C(7), C(8)−C(9), and C(11)−C(12) bonds, whereas the LUMO orbitals are bonding in these regions. As a result, we can expect the contraction of these bond lengths. The data in Table 2 confirm that these inter-ring bond lengths become considerably shorter in the excited state as discussed earlier. On the contrary, the HOMO orbitals are bonding across the C(2)−C(3), C(3)−C(4), C(5)−C(6), C(6)−C(1), C(7)−C(8), C(9)−C(10), C(10)−C(11),

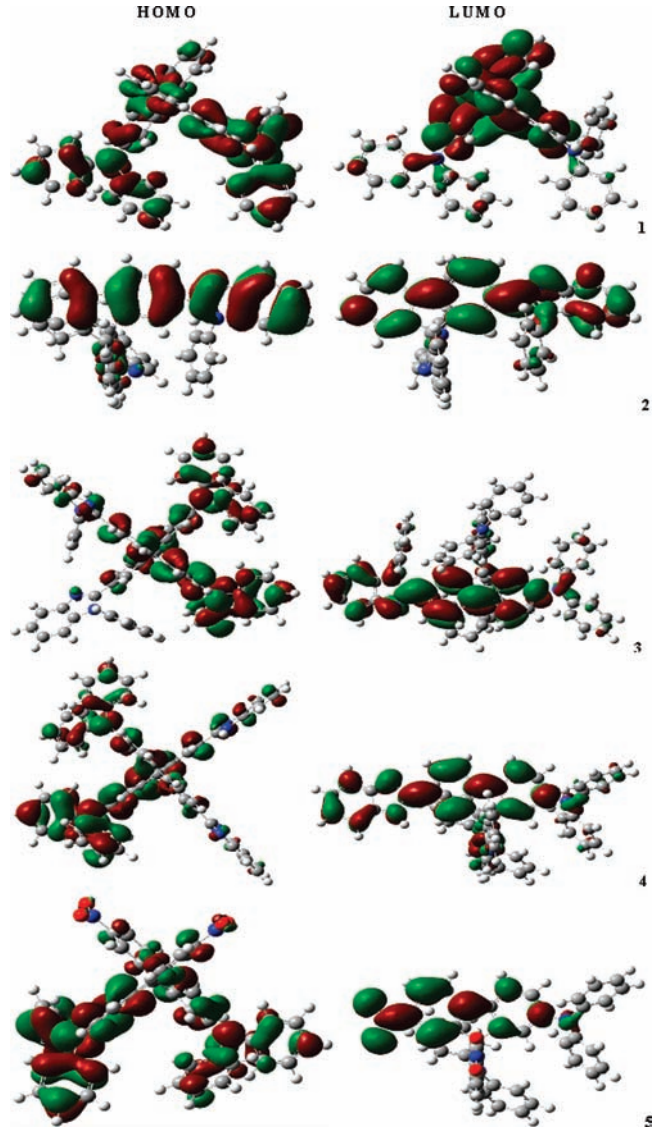

Figure 3. Plots of HOMO and LUMO of 1−5 by DFT//B3LYP/6-31G(d).

TABLE 3: Negative of the HOMO ($-\varepsilon_{HOMO}$) and LUMO Energies ($-\varepsilon_{LUMO}$), HOMO−LUMO Gaps Calculated by DFT and the Lowest Excited Energies Calculated by TD-DFT in eV for 1−5

molecule	$-\varepsilon_{HOMO}$	$-\varepsilon_{HOMO}$ (exptl)	$-\varepsilon_{LUMO}$	$-\varepsilon_{LUMO}$ (exptl)	ΔE_{H-L}	E_g	E_g (exptl)
1	4.83	5.43	0.86	2.26	3.97	3.47	3.17
2	5.41	5.73	1.39	2.43	4.02	3.58	3.30
3	4.88	5.46	1.37	2.63	3.51	3.08	2.86
4	4.95		1.51		3.44	3.02	
5	5.27		2.38		2.89	2.48	

TABLE 4: Ionization Potentials, Electronic Affinities, Extraction Potentials, and Reorganization Energies for Each Molecule (in eV) Calculated by DFT//B3LYP/6-31G(d)

molecule	IP(v)	IP(a)	HEP	EA(v)	EA(a)	EEP	λ_{hole}	$\lambda_{electron}$
1	5.82	5.77	5.72	0.22	0.09	0.04	0.10	0.18
2	6.47	6.38	6.29	0.34	0.48	0.61	0.18	0.27
3	5.76	5.71	5.66	0.44	0.61	0.77	0.10	0.33
4	5.83	5.78	5.73	0.57	0.70	0.83	0.10	0.26
5	6.25	6.21	6.17	1.19	1.37	1.54	0.08	0.35

and C(12)−C(7) bonds but the LUMO orbitals have nodes in these regions. The calculated results in Table 2 are in agreement with this anticipated elongation of these bonds.

From Figure 4 and Table 3, it can be seen that, the calculated HOMO and LUMO energies and the lowest excited energies (E_g) have the same variation trends with the experimental data. As shown, the HOMO energy in 1 is very large and the LUMO energy in 2 is very small, indicating that the introduction of diphenylamino as electron donor (D) in 1 and diphenylbenzimidazole as electron acceptor (A) in 2 has largely improved their hole-creating and electron-accepting ability, respectively. Therefore, the incorporation of these D and A moieties in 3 will improve both the hole- and electron-creation abilities, which is confirmed by the large HOMO energy (−4.88 eV) and low LUMO energy (−1.37 eV) of 3 in Table 3. By replacing diphenylbenzimidazole with nitryl and benzimidazole, we find that the HOMO energies are a little smaller and the LUMO energies largely decreased in 4 (−4.95, −1.51 eV) and 5 (−5.27, −2.38 eV) than that of 3. This implies that 4 and 5 are nice electron-injection materials.

For the purpose of more easily observing the variations of HOMOs, LUMOs, and energy gaps, sets of one-electron energy levels of 1−5 (from HOMO-3 to LUMO+3) are plotted in Figure 5. It can be seen that the energy difference between HOMO and HOMO-1, and LUMO and LUMO+1 for 1 (0.03, 0.01 eV), 2 (0.21, 0.06 eV), 3 (0.04, 0.07 eV), 4 (0.03, 0.01 eV), and 5 (0.03, 0.01 eV) is very small. This suggests that it is possible for the promotion of an electron from the HOMO-1 to LUMO, HOMO to LUMO+1, or HOMO-1 to LUMO+1, except the HOMO → LUMO transition (Absorption and Emission Spectra section).

It can also be found in Table 3 that the HOMO−LUMO gaps (ΔE_{H-L}) have the same variation trend with the optical band gaps (E_g). The energy gaps of 4 and 5 are both smaller than that of 3, consistent with the slightly decreased HOMO energies and the largely reduced LUMO energies of 4 and 5 compared with that of 3. From this we can predict the red-shifted absorption and emission wavelengths in 4 and 5. The investigation in this section indicates that the HOMOs, LUMOs, and energy gaps of these spirobifluorene derivatives are affected by the use of various D and A moieties. It can be found that 3 is a nice hole- and electron-acceptance material and 4 and 5 are good electron-injection molecules.

3.3. Ionization Potentials and Electron Affinities. As the device performance of OLEDs depends on the charge injection, transfer, and balance as well as the exciton confinement in a device. It is necessary to investigate the ionization potential (IP) and electron affinity (EA), which can be used to evaluate the energy barrier for the injection of holes and electrons. The DFT-calculated IP, EA, as well as hole extraction potential (HEP) and electron extraction potential (EEP) for 1−5 are listed in Table 4. The IP and EA can be either for vertical excitations (v, at the geometry of the neutral molecule) or adiabatic excitations (a, optimized structure for both the neutral and charged molecule). In addition, HEP is the energy difference from M (neutral molecule) to M^+ (cationic), with using M^+ geometric structure in calculation, and EEP is the energy

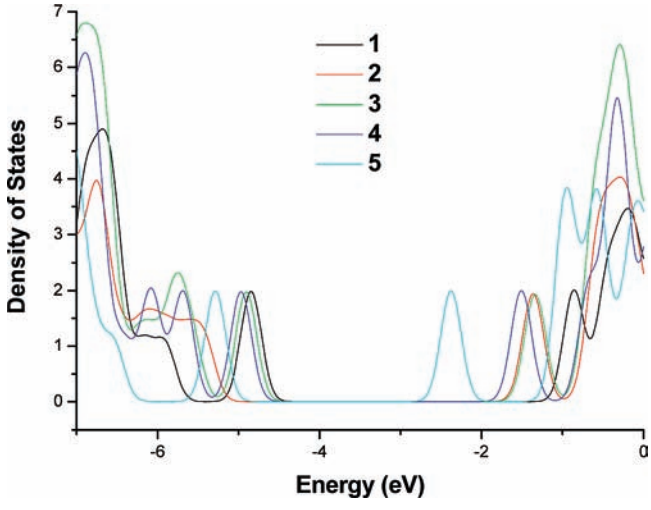

Figure 4. Total of density of states of 1−5.

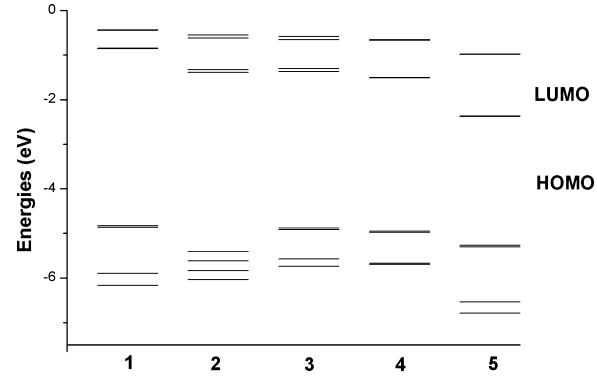

Figure 5. Sets of one-electron energy levels of 1−5 by DFT//B3LYP/6-31G(d).

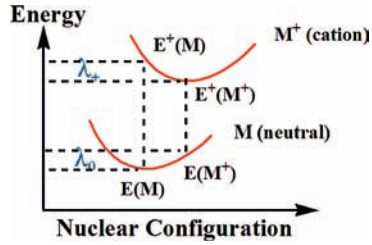

Figure 6. Internal reorganization energy for hole transfer.

difference from M to M^- (anionic), with using M^- geometric structure in calculation.

As shown in Table 4, the small value of the IP for 1 (5.82 eV) and the large value of the EA for 2 (0.48 eV) demonstrate that the incorporation of diphenylamino can improve the hole-creating ability in 1, and the introduction of diphenylbenzimidazole benefits the electron-accepting ability in 2. As a result, the combination of both of them in 3 may favor the hole- and electron-injection abilities, suggested by the decreased IP (5.76 eV) and increased EA (0.61 eV) values of 3 in Table 4. This is consistent with the investigation of the HOMO and LUMO energies discussed above. In addition, the EA values of 4 and 5 are both larger than that of 3, indicating that the substituent of diphenylbenzimidazole with nitryl and benzimidazole greatly improves the electron-acceptance capability. This also confirms the discussion of the HOMO and LUMO energies and provides an in-depth interpretation of the electronic properties of these spirobifluorene derivatives.

To value the charge transfer (or transport) rate and balance, reorganization energy (λ) was calculated for the studied molecules. Generally, organic π-conjugated materials are assumed to transport charge at room temperature via a thermally activated hopping-type mechanism.[19−22] The hole- and electron-transfer process between adjacent spatially separated segments can be summarized as follows:

$$M^+ + M \rightarrow M + M^+$$

$$M^- + M \rightarrow M + M^-$$

where M represents the neutral species undergoing charge transfer, and the M^+/M^- species contains the hole/electron. If the temperature is sufficiently high to treat vibrational modes classically, then the standard Marcus/Hush model yields the following expression for the hole (or electron) charge transfer rate,[23−26] assuming that hole/electron traps are degenerate:

$$\kappa_{\text{hole/electron}} = \left(\frac{\pi}{\lambda k_B T}\right)^{1/2} \frac{V^2}{\hbar} \exp\left(-\frac{\lambda}{4 k_B T}\right) \qquad (1)$$

where T is the temperature, k_B is the Boltzmann constant, λ is the reorganization energy due to geometric relaxation accompanying charge transfer, and V is the electronic coupling matrix element between the two species, dictated largely by orbital overlap. Obviously, λ and V are the two most important parameters and have a dominant impact on the charge-transfer rate, especially the former. Then we mainly investigate the reorganization energy for 1−5. Here, the reorganization energy is just the internal reorganization energy of the isolated active organic π-conjugated systems due to ignoring any environmental relaxation and changes. Hence, the reorganization energy for hole/electron transfer in eq 1 can be defined as[22]

$$\begin{aligned}\lambda_{\text{hole}} = \lambda_+ + \lambda_0 = [E^+(M) - E^+M^+)] + \\ [E(M^+) - E(M)] = \\ [E^+(M) - E(M)] - [E^+(M^+) - E(M^+)] = \\ IP(v) - HEP\end{aligned} \qquad (2)$$

$$\begin{aligned}\lambda_{\text{electron}} = \lambda_- + \lambda_0 = [E^-(M) - E^-(M^-)] + \\ [E(M^-) - E(M)] = \\ [E(M^-) - E^-(M^-)] - [E(M) - E^-(M)] = \\ EEP - EA(v)\end{aligned} \qquad (3)$$

As illustrated in Figure 6, E(M) and $E^+(M^+)/E^-(M^-)$ represent the energies of the neutral and cation/anion species in their lowest energy geometries respectively, whereas $E(M^+)/E(M^-)$ and $E^+(M)/E^-(M)$ represent the energies of the neutral and cation/anion species with the geometries of the cation/anion and neutral species, respectively. This description holds as long as the potential-energy surfaces are harmonic and the λ_0 and λ_+/λ_- terms are close in energy. As it is known that many factors, including heteroatom identity, heterocycle substituents, and conjugation length, are important in dictating the reorganization energy.

For emitting-layer materials, it needs to achieve the balance between hole injection and electron acceptance. Furthermore, the lower the λ values, the bigger the charge-transport rate. The data in Table 4 show that the λ_{hole}'s for 1−5 are all smaller than their respective $\lambda_{\text{electron}}$'s, suggesting that the hole transfer rate is higher than the electron transfer rate. Furthermore, the small λ_{hole}'s and $\lambda_{\text{electron}}$'s for 1 (0.10, 0.18), 2 (0.18, 0.27), and 3 (0.10, 0.33) indicate that they are nice charge transfer materials. To further improve the charge transportation, 4 and 5 were designed. The $\lambda_{\text{electron}}$ (0.26) of 4 and λ_{hole} (0.08) of 5 are all smaller than that of 3, implying that 4 has a higher electron transfer rate and 5 has a higher hole transfer rate than that of 3, respectively. Therefore, 4 and 5 are better emitting materials with high quantum efficiency. In addition, the difference between the λ_{hole} and $\lambda_{\text{electron}}$ for 4 (0.16 eV) is smaller than that of 3 (0.23 eV), suggesting that the designed molecule 4 has better hole- and electron-transporting balance and can act as a nice ambipolar material.

3.4. Absorption and Emission Spectra. TD-DFT//B3LYP/6-31G(d) has been employed on the basis of the optimized geometry to investigate the absorption and emission spectra of 1−5. The transition energies, oscillator strengths, and main configurations for the most relevant singlet excited states in each molecule are listed in Tables 5 and 6, respectively. For the absorption spectra, the calculated data for 1−3 have good agreement with the experimental results, with the largest deviation of 5 nm. All of the electronic transitions are of $\pi \rightarrow \pi^*$ type, and the strongest absorption peaks with largest oscillator strengths for 1−5 arise from $S_0 \rightarrow S_1$, $S_0 \rightarrow S_2$, $S_0 \rightarrow S_3$, $S_0 \rightarrow S_4$, and $S_0 \rightarrow S_4$ respectively, which mainly correspond to the promotion of an electron from HOMO to LUMO+1, HOMO to LUMO, and HOMO-1 to LUMO. As shown in Table 5, the absorption spectra exhibit red shifts to some extent from 3 (391.37 nm) to 4 (400.55 nm) and from 3 to 5 (468.37 nm) due to the substituent of diphenylbenzimidazole with nitryl and benzimidazole, which confirms the prediction from the energy gap discussed above. It is known that the transition moment is proportional to the oscillator strength[27] for an electronic transi-

TABLE 5: Electronic Transition Data Obtained by TD-DFT ($\lambda_{abs,max}$) for 1−5 at the B3LYP/6-31G(d) Optimized Geometry

molecule	electronic transitions	$\lambda_{abs,max}$ (nm)	exp[a] λ_{abs}	f	transition moment	main configurations	
1	$S_0 \rightarrow S_1$	357.12	352	0.3855	2.00	HOMO-1 → LUMO+1	0.23
						HOMO → LUMO	0.62
						HOMO → LUMO+1	0.12
2	$S_0 \rightarrow S_1$	346.26		0.0460		HOMO → LUMO	0.70
	$S_0 \rightarrow S_2$	336.01	331	0.6523	2.38	HOMO-1 → LUMO	0.11
						HOMO-1 → LUMO+1	0.16
						HOMO → LUMO+1	0.64
3	$S_0 \rightarrow S_1$	402.26		0.1789		HOMO → LUMO	0.69
	$S_0 \rightarrow S_3$	391.37	386	0.6590	2.89	HOMO-1 → LUMO	0.34
						HOMO-1 → LUMO+1	0.16
						HOMO → LUMO+1	0.57
4	$S_0 \rightarrow S_1$	410.72		0.0908		HOMO-1 → LUMO	0.16
						HOMO → LUMO	0.66
						HOMO → LUMO+1	0.13
	$S_0 \rightarrow S_4$	400.55		0.8994	3.33	HOMO-1 → LUMO	0.61
						HOMO → LUMO+1	0.26
5	$S_0 \rightarrow S_1$	499.03		0.0036		HOMO-1 → LUMO	0.37
						HOMO → LUMO	0.60
	$S_0 \rightarrow S_4$	468.37		0.3995	0.28	HOMO-1 → LUMO	0.42
						HOMO-1 → LUMO+1	0.30
						HOMO → LUMO	0.22
						HOMO → LUMO+1	0.38

[a] Measured in tetrahydrofuran (Ref. 14).

TABLE 6: Emission Data Obtained by TD-DFT for 1−5 at the CIS/3-21G(d) Optimized Geometry

molecule	electronic transitions	λ^{em} (nm)	exp[a]	f	E_{Flu} (ev)	E_b (ev)	main configurations		τ (ns)
1	$S_1 \rightarrow S_0$	383.41	394	0.5886	3.23	0.74	HOMO → LUMO	0.64	3.76
2	$S_1 \rightarrow S_0$	388.42	383	0.9745	3.19	0.83	HOMO → LUMO	0.63	2.33
3	$S_1 \rightarrow S_0$	436.12	445	1.1693	2.84	0.67	HOMO → LUMO	0.65	2.45
4	$S_1 \rightarrow S_0$	438.18		1.2072	2.83	0.61	HOMO-1 → LUMO	0.14	2.39
							HOMO → LUMO	0.64	
5	$S_1 \rightarrow S_0$	475.11		0.3428	2.61	0.28	HOMO-1 → LUMO+1	0.20	9.90
							HOMO → LUMO+1	0.65	

[a] Measured in tetrahydrofuran (Ref. 14).

tion and reflects the transition probability from the ground state to the excited state. The transition moments and the largest oscillator strength in 3−5 (3, 2.89, 0.6590; 4, 3.33, 0.8994; 5, 0.28, 0.3995) indicates that the transition probabilities becomes higher in the order 5 → 3 → 4.

For the emission spectra, the emission peaks with the largest oscillator strength for 1−5 are all assigned to $\pi \rightarrow \pi^*$ character, arising from the S_1, HOMO → LUMO transition. As in the case of the absorption spectra, the emission wavelengths for 4 and 5 exhibit red shifts compared with that of 3. The Stokes shifts ranging from 7 to 52 nm may be explained by a more planar conformation of the excited state of the considered oligomers. Also, the high oscillator strengths of the $S_1 \rightarrow S_0$ transitions and the largest emission wavelengths (436.12, 438.18, 475.11 nm) for 3, 4, and 5 imply that they can be used as efficient blue-light-emitting materials.

Table 6 also lists the emission lifetimes (τ) calculated for spontaneous emission by using the Einstein transition probabilities according to the formula (in au)[28,29]

$$\tau = \frac{c^3}{2(E_{Flu})^2 f} \quad (6)$$

where c is the velocity of light, E_{Flu} is the transition energy, and f is the oscillator strength. The data of E_{Flu} and f are also showed in Table 6. The calculated lifetimes for the spirobifluorene derivatives are 3.76 (1), 2.33 (2), 2.45 (3), 2.39 (4), and 9.90 (5) ns, indicating that, by replacing diphenylbenzimidazole with nitryl and benzimidazole, the radiative lifetime increases and decreases, respectively. Here, the discussion further supports the influence of different D and A moieties on the biphenyl branches of the spirobifluorene.

It is well-known that fluorescence emission is accompanied with energy rejection, that is to say, $h\nu = E_{Flu}$. Here, $E_{Flu} = \Delta E_{H-L} - E_b$, and E_b is the exciton binding energy. As shown in Table 6, the values of E_b for 1−5 indicate that the energy required to destroy a hole−electron exciton follows the order 5 (0.28 eV) < 4 (0.61 eV) < 3 (0.67 eV) < 1 (0.74 eV) < 2 (0.83 eV). This implies that it becomes easier to destroy the hole−electron excitons following the order 2 → 1 → 3 → 4 → 5, and our designed molecule 5 has the smallest exciton binding energy.

4. Conclusions

Because of great potential for application in organic light-emitting diodes, a series of spirobifluorene derivatives have been systematically investigated in this work. Necessarily, the structures in the ground state have been compared with those of the excited state to trace the structural variations. The calculated results show that their optical and electronic properties, including HOMOs, LUMOs, energy gaps, ionization potentials, electron affinities, reorganization energies, absorption, and emission spectra, as well as exciton binding energies, are affected by the different D and A moieties of these spirobifluorene derivatives. By the introduction of diphenylamino and

diphenylbenzimidazole in the spirobifluorene (3), the HOMO energies, electron affinities increase, the LUMO energies, ionization potentials, reorganization energies, and exciton binding energies decrease, the energy gap becomes narrow, and the absorption and emission spectra exhibit red shifts to some extent. By replacing diphenylbenzimidazole with benzimidazole (4) and nitryl (5), the ionization potentials and electron affinities increase, the HOMO and LUMO energies, reorganization energies, and exciton binding energies decrease, the energy gaps also become narrow, and the absorption and emission spectra show small red shifts. This indicates that 3 and the designed molecules (4 and 5) are excellent charge injection and transportation materials with large fluorescent intensity. Importantly, the emission spectra of the studied molecules 3 (436.12 nm), 4 (438.18 nm), and 5 (475.11 nm) display in the range of the blue spectrum. Finally, it can be obtained from the calculated results that the investigated ambipolar spirobifluorene derivatives (3, 4, and 5) can be used as efficient blue-light-emitting materials in organic light-emitting diodes. Also, the calculated results indicate that the designed molecules 4 and 5 are good electron and hole transfer materials respectively and have nice photophysical properties. As a result, we are convinced that our work should contribute to orientate the synthesis efforts and help understand the structure−properties relation of these materials.

Acknowledgment. This work is supported by the Major State Basic Research Development Program (2002CB 613406), the National Natural Science Foundation of China (Project No. 20673045), and the Open Project of State Key Laboratory of Supramolecular Structure and Materials of Jilin University (SKLSSM200716).

References and Notes

(1) Saragi, T. P. I.; Spehr, T.; Siebert, A.; Fuhrmann-Lieker, T.; Salbeck, J. *Chem. Rev.* **2007**, *107*, 1011–1065.

(2) Pudzich, R.; Salbeck, J. *Synth. Met.* **2003**, *138*, 21–31.

(3) Lin, H.-W.; Ku, S.-Y.; Su, H.-C.; Huang, C.-W.; Lin, Y.-T.; Wong, K.-T.; Wu, C.-C. *Adv. Mater.* **2005**, *17*, 2489–2493.

(4) Shirota, Y.; Kinoshita, M.; Noda, T.; Okumoto, K.; Ohara, T. *J. Am. Chem. Soc.* **2000**, *122*, 11021–11022.

(5) Zhu, Y.; Kulkarni, A. P.; Jenekhe, S. A. *Chem. Mater.* **2005**, *17*, 5225–5227.

(6) Chen, C.-T.; Lin, J.-S.; Moturu, M. V. R. K.; Lin, Y.-W.; Yi, W.; Tao, Y.-T.; Chen, C.-H. *Chem. Commun.* **2005**, *16*, 3980–3982.

(7) Xu, X.; Chen, S.; Yu, G.; Di, C.; You, H.; Ma, D.; Liu, Y. *Adv. Mater.* **2007**, *19*, 1281–1285.

(8) Haung, T.-H.; Lin, J.-T.; Chen, L.-Y.; Lin, Y.-T.; Wu, C.-C. *Adv. Mater.* **2006**, *18*, 602–606.

(9) Li, Z. H.; Wong, M. S.; Fukutani, H.; Tao, Y. *Org. Lett.* **2006**, *8*, 4271–4274.

(10) Habrard, F.; Ouisse, T.; Stephan, O.; Aubouy, L.; Gerbier, P.; Hirsch, L.; Huby, N.; Vander Lee, A. *Synth. Met.* **2006**, *156*, 1262–1270.

(11) Lee, T. H.; Tong, K. L.; So, S. K.; Leung, L. M. *Synth. Met.* **2005**, *155*, 116–124.

(12) Chien, Y.-Y.; Wong, K.-T.; Chou, P.-T.; Cheng, Y.-M. *Chem. Commun.* **2002**, 2874–2875.

(13) Ku, S.-Y.; Cheng, Y.-M.; Lin, X.-Y.; Hung, Y.-Y.; Pu, S.-C.; Wong, K.-T.; Chou, P.-T.; Lee, G.-H. *J. Org. Chem.* **2006**, *71*, 456–465.

(14) Liao, Y.-L.; Lin, C.-Y.; Wong, K.-T.; Hou, T.-H.; Hung, W.-Y. *Org. lett.* **2007**, 4511–4514.

(15) Frisch, M. J.; Trucks, G. W.; Schlegel, H. B.; Scuseria, G. E.; Robb, M. A.; Cheeseman, J. R.; Montgomery, J. A., Jr.; Vreven, T.; Kudin, K. N.; Burant, J. C.; Millam, J. M.; Iyengar, S. S.; Tomasi, J.; Barone, V.; Mennucci, B.; Cossi, M.; Scalmani, G.; Rega, N.; Petersson, G. A.; Nakatsuji, H.; Hada, M.; Ehara, M.; Toyota, K.; Fukuda, R.; Hasegawa, J.; Ishida, M.; Nakajima, T.; Honda, Y.; Kitao, O.; Nakai, H.; Klene, M.; Li, X.; Knox, J. E.; Hratchian, H. P.; Cross, J. B.; Adamo, C.; Jaramillo, J.; Gomperts, R.; Stratmann, R. E.; Yazyev, O.; Austin, A. J.; Cammi, R.; Pomelli, C.; Ochterski, J. W.; Ayala, P. Y.; Morokuma, K.; Voth, G. A.; Salvador, P.; Dannenberg, J. J.; Zakrzewski, V. G.; Dapprich, S.; Daniels, A. D.; Strain, M. C.; Farkas, O.; Malick, D. K.; Rabuck, A. D.; Raghavachair, K.; Foresman, J. B.; Ortiz, J. V.; Cui, Q.; Baboul, I.; Martin, R. L.; Fox, D. J.; Keith, T.; Al-Laham, M. A.; Peng, C. Y.; Nanayakkara, A.; Challacombe, M.; Gill, P. M. W.; Johnson, B.; Chen, W.; Wong, M. W.; Gonzalez, C.; Pople, J. A. *Gaussian 03*, Rev. B.04; Gaussian, Inc.: Pittsburgh, PA, 2003.

(16) Hay, P. J. *J. Phys. Chem. A* **2002**, *106*, 1634–1641.

(17) Curioni, A.; Andreoni, W.; Treusch, R.; Himpsel, F. J.; Haskal, E.; Seidler, P.; Heske, C.; Kakar, S.; van Buren, T.; Terminello, L. *J. Appl. Phys. Lett.* **1998**, *72*, 1575–1577.

(18) Hong, S. Y.; Kim, D. Y.; Kim, C. Y.; Hoffmann, R. *Macromolecules* **2001**, *34*, 6474–6481.

(19) Epstein, A. J.; Lee, W. P.; Prigodin, V. N. *Synth. Met.* **2001**, *117*, 9.

(20) Reedijk, J. A.; Martens, H. C. F.; van Bohemen, S. M. C.; Hilt, O.; Brom, H. B.; Michels, M. A. J. *Synth. Met.* **1999**, *101*, 475–476.

(21) Mott, N. F.; Davis, E. A. *Electronic Processes in Non-Crystalline Materials*, 2nd ed.; Oxford University Press: Oxford, 1979.

(22) Hutchison, G. R.; Ratner, M. A.; Marks, T. J. *J. Am. Chem. Soc.* **2005**, *127*, 2339–2350.

(23) Marcus, R. A. *Rev. Mod. Phys.* **1993**, *65*, 599–610.

(24) Marcus, R. A.; Eyring, H. *Annu. Rev. Phys. Chem.* **1964**, *15*, 155–196.

(25) Hush, N. S. *J. Chem. Phys.* **1958**, *28*, 962–972.

(26) Marcus, R. A. *J. Chem. Phys.* **1956**, *24*, 966–978.

(27) Peyerimhoff, S. D. In *The Encyclopedia of Computational Chemistry*; Schleyer, P. von R., Allinger, N. L., Clark, T., Gasteiger, J., Kollman, P. A., Schaefer, H. F., III, Schreiners, P. R., Eds.; Wiley: Chichester, U.K., 1998; pp 2646−2664.

(28) Litani-Barzilai, I.; Bulatov, V.; Schechter, I. *Anal. Chim. Acta* **2004**, *501*, 151–156.

(29) Lukeš, V.; Aquino, A.; Lischka, H. *J. Phys. Chem. A* **2005**, *109*, 10232–10238.

JP903511R